The Temperature Role in the Manufacturing of an Electrode for Supercapacitors with Carbon Black and Graphene Oxide

Mario Rapisarda[a], Achille Damasco[b,*], Giancarlo Abbate[b], Michele Meo[a]

[a]Department of Mechanical Engineering, University of Bath, Bath, BA2 7AY, UK
[b]Dipartimento di Scienze Fisiche "Ettore Pancini", Università degli Studi di Napoli "Federico II", Via Cintia 21, 80126, Napoli, Italia
achille.damasco@unina.it

Supercapacitors (SCs) are energy storage devices with a growing interest thanks to their high-power charge and discharge process and long-cycle life. Their main drawback, when compared to more common devices such as batteries, consists in a low energy density. The performances of SCs can however be improved with the coupling of additives to the main active material, which usually is an Activated Carbon. The most common additive is instead Carbon Black (CB), while more recently also Graphene-derived materials have been successfully exploited for this purpose, as the reduced Graphene Oxide (rGO). However, besides raw materials choice, details related to the manufacturing have a leading importance in the attempt to obtain novel active materials with an industrial-ready process which also looks toward the needs of more environmental friendly and economically convenient solutions. In this work, a physical-chemical analysis is performed to show temperature effects on CB, GO and on a CB/GO water-based slurry with helpful results about GO reduction and CB/GO nanocomposite formation.

1. Introduction

The research for a scalable solution for complex devices like supercapacitors (SCs) involves a wide amount of constraints, which regard costs control, scalability of the manufacturing process and the environmental impact. These involve different subjects of focus for the scientific research, where two main branches can be identified: raw materials choice and optimization of the manufacturing process. The most common active material for commercial SC electrodes is Activated Carbon (AC) (Frackowiak, Beguin, 2001), which can be improved with conductive additives as Carbon Black (CB) (Carmo et al., 2007). For the development of innovative SCs, in the recent literature the reduced Graphene Oxide (rGO) is found to be an excellent candidate as an alternative additive (Ke, Wang, 2016). It consists of a graphene-like material that derives from the treatment of Graphene Oxide (GO), which is the exfoliated form of Graphite Oxide (GtO) (Stobinski et al., 2014). In the branch of manufacturing, thermal treatments (i.e., application of controlled temperatures) have different roles: in electrode fabrication, they are required to dry and, in case, recover the solvent from the slurry after its coating on current collectors; they may be used to cause and/or accelerate chemical reactions to fully develop active materials properties. Since these effects can take place at the same time, the temperature choice becomes crucial to guarantee an optimized process. Particularly, for the CB and/or GO water-based slurries under examination in this study, a temperature that ensure a quick and complete evaporation of water and a quick and effective thermal reduction of GO to rGO (Jeong et al., 2009) must be found. For the latter, even though chemical reduction techniques were also successfully exploited with promising result (Pei et al., 2010), thermal ones can be preferred because, in a scale-up analysis, it does not imply the addition in the slurry of a component that does not strictly belong to the final electrode. This is important because the introduction of new components, which can potentially be expensive and dangerous for the environment, to an industrial scale for the manufacturing of new commercial devices should be limited.

In this work, a physical-chemical analysis was performed to describe the multiple effects of temperature on CB and GO in the manufacturing of a SC electrode. Two thermal treatment temperatures, specifically of 200 °C and 550 °C, were chosen to study their different effects on the samples in order to achieve a manufacturing

process optimization, while an ambient drying (at 20 °C) was performed as reference. CB and GO were studied both separately and as a nanocomposite electrode (CB/GO), together with the adopted surfactant, Triton X-100 (TX100). In CB/GO, the thermally reduced GO becomes a conductive binder that can actively contribute to the electrochemical properties (Rapisarda et al., 2020). Differently from our previous work (Rapisarda et al., 2020), and besides the analysis conducted at three different temperatures, this study also focuses on the GO reduction process thanks to a Zeta Potential test.

2. Experimental section

2.1 Slurry preparation

CB powder (Black Pearls® 2000) was supplied by Cabot Corporation, TX100 (Laboratory Grade) was purchased from Sigma-Aldrich and GtO powder was acquired from XIAMEN TOB NEW ENERGY TECHNOLOGY Co. Deionized water (MilliQ®) was used throughout all the experiments. All chemicals were used as received without further purification.

A CB-only slurry (50 mg mL^{-1}) was prepared adding CB powder to a solution of water and TX100 and mixed as follows: 30 min of bath ultrasonication followed by 2 h of magnetic stirring. A specific amount of TX100 was pre-mixed in water through bath ultrasonication so that its concentration with respect of the CB is the 3 wt.%.

A part of the resulting CB-only slurry was mixed with a GO dispersion in water (8 mg mL^{-1}) with the aid of an ultrasonic bath. A homogeneous CB/GO slurry (with a final concentration of 34 mg mL^{-1}) was finally obtained after 12 h of further mixing using a magnetic stirrer. The volume of the GO dispersion in water, previously obtained by ultrasonic exfoliation of GtO in water, was fixed in order to achieve a mass ratio of GO:CB=1:10.

2.2 Sample preparation

Thermally treated samples were obtained starting from the doctor blead coating of the different slurries on an Aluminum substrate and then subjected to the three different conditions: ambient drying at 20 °C (AD), heating up to 200 and 550 °C in a tubular furnace for 1 h under Argon atmosphere (respectively TT_200 and TT_550). Powdered samples of the coatings were finally collected scratching the substrate and stored in a dry atmosphere before subsequent analysis.

2.3 Physical-chemical analysis

Particles of CB and CB/GO samples were imaged through Transmission Electron Microscopy (TEM, JEOL JEM-2100Plus). The powdered samples were first dispersed in ethanol and sonicated (in ultrasonic bath for 10 min) and then drop-casted on TEM grids.

Raman Spectroscopy (RS) was used to analyse the chemical structure of CB and CB/GO samples using an inVia Raman Microscope by Renishaw, with a 523 nm laser source (IK Series He-Cd).

The crystalline structure was instead analysed with X-Ray Diffractometry (XRD) in a STADI P diffractometer by STOE equipped with a Cu-Kα generator (1.54 Å of wavelength). The interplanar spacing (d) in crystal lattices and the crystallite size (L) were obtained from the data using, respectively, Bragg's law (Bragg W. H., Bragg W. L., 1913) and Scherrer equation (Scherrer, 1918):

$$d = \frac{\lambda}{2 \cdot \sin\theta} \tag{1}$$

$$L = \frac{K\lambda}{B \cdot \cos\varphi} \tag{2}$$

where λ is the radiation wavelength, θ is the scattering angle of the corresponding lattice, K is a shape factor, B is the line broadening at half maximum intensity of the peak, φ is the corresponding scattering angle.

The ζ-potential on GO and on GO_TT_550 samples was measured using a Malvern Zetasizer Nano system, with irradiation from a 633 nm He-Ne laser. GO was diluted from 8 mg mL^{-1} to 30 μg mL^{-1} to allow water transparency, while GO_TT_550 powder was dispersed in water (30 μg mL^{-1}), mixed for 30 min and bath sonicated for 30 min. The diluted samples were injected in folded capillary cells and tested at 25 °C. The Zetasizer performs a combination of electrophoresis and laser Doppler velocimetry techniques to measure the electrophoretic mobility (μ) of the particles. From the measure of μ, this analysis provides a measure of the ζ-potential through the Henry's equation (Henry, 1931) in the so-called Huckle and Smoluchowsky limits (Delgrado, 2005):

$$\mu = \frac{2\varepsilon\zeta f(ka)}{3\eta} \tag{3}$$

where ε is the dielectric constant of the solvent, η is its viscosity and *f(ka)* is a function that varies smoothly from 1.0 to 1.5 in this experiment limits (i.e., for water-based slurry and with particles size above 100 nm).

3. Results and discussion

3.1 TEM Imaging

The behavior of CB particles subjected to different temperatures conditions, and the effects of their mixing with GO was initially studied with TEM imaging. According to ASTM definition (ASTM Standard D30530-20a), CB particles show a peculiar hierarchical morphology with spherical nodules, having sizes ranging from 10 to 300 nm, being the fundamental building block. These form at first aggregates of 85-500 nm, held together by covalent bonds, and secondarily agglomerates of 1-100 µm thanks to van der Waals interactions. Figure 1a shows a TEM image of a large agglomerate from the CB_AD sample with a higher magnification in the onset: the size-scales of nodules, aggregates and agglomerates are in good agreement with the previous definition. This structure is well maintained also for both the thermally treated samples, CB_TT_200 and CB_TT_550 (with the latter being pictured in Figure 1b), proving CB inertness at the tested conditions and thus simplifying the thermal treatment optimization. When introduced into the slurry, GO interacts with CB leading to a 3D carbonaceous network aided by the TX100 presence in solution. Particularly, it allows an initial dispersion of CB particles in water that are subsequently surrounded by GO sheets, as observable in TEM images in Figure 1c-e from, respectively, CB/GO_AD, CB/GO_TT_200 and CB/GO_TT_550 samples. Additionally, it is possible to notice the reduction of GO to rGO thanks to the appearance of interference lines in the large sheets, as highlighted from the high magnification image from the CB/GO_TT_550 sample in Figure 1f.
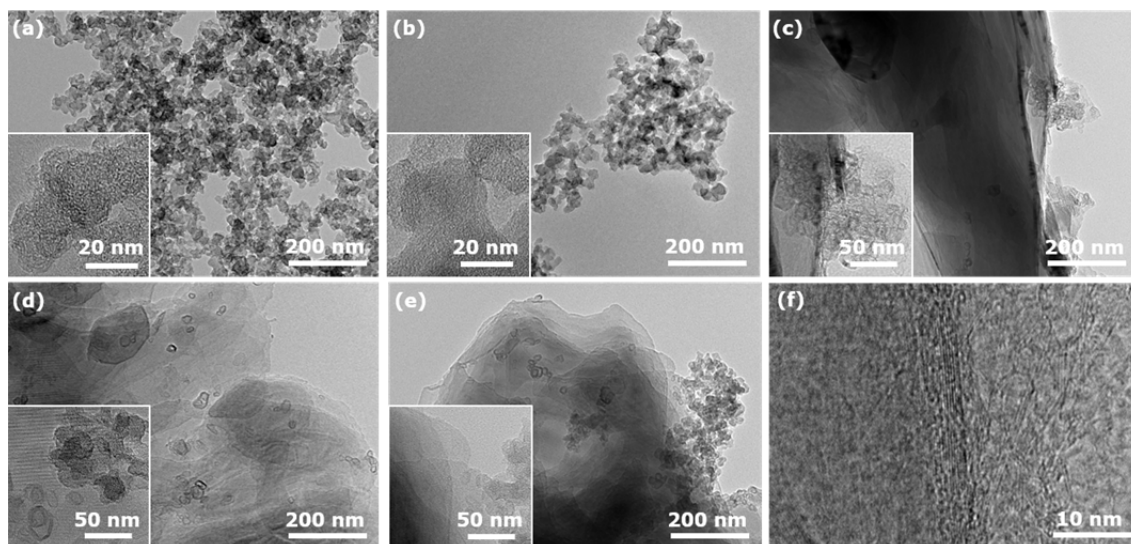

Figure 1: TEM images of (a) CB_AD, (b) CB_TT_550, (c) CB/GO_AD, (d) CB/GO_TT_200, and (e) CB/GO_TT_550 with higher magnification in the onset and (f) high magnification image of rGO sheets.

3.2 RS and XRD characterization

The resulting spectra from Raman characterization of CB and CB/GO samples are shown in Figure 3a. Being carbonaceous materials, they all show the D band at ~1,348 cm^{-1} and the G band at ~1,605 cm^{-1} and also 2nd order scatterings between 2,600 and 3,000 cm^{-1}. While the first two features arise from, respectively, the breathing modes of sp^2 hybridized carbon atoms due to a defective crystalline structure and the primary vibration modes of the sp^2 atoms, the third one indicates turbostratic arrangements of graphene layers (Pimenta at al. 2007). The peaks intensity ratio of the D and G bands (I_D/I_G) is proportional with the disorder induced by defects in carbon atoms lattices, allowing thus the evaluation of structure quality (Ferrari, 2007). As evidenced from the values summarized in Table 1, the introduction of GO in the slurry leads to a reduction of I_D/I_G from 1.07 of CB only to 0.96 for CB/GO, with both subjected to ambient drying. This confirms the interaction of GO sheets with CB particles, which was previously observed with TEM imaging, and thus GO role as dispersing agent leading to a homogeneous carbonaceous nanocomposite. Furthermore, also the effects of the thermal treatments on I_D/I_G can be observed: while no differences are shown for CB only samples, explainable with CB inertness at the tested treatment conditions, in CB/GO ones the I_D/I_G value

increases from 0.96 of the ambient dried sample to 1.05 and 1.04 of, respectively, the 200 and 550 °C treated samples. Such increase of disorder is a consequence of topological defects induced on graphene lattices after the release of Carbon Dioxide, Carbon Monoxide and water vapor driven by heat provision, which is the mechanism governing the reduction of GO (Schniepp et al, 2007). The slightly lower value shown in CB/GO_TT_550 could be explained with a tendency of the structure to rearrange thanks to the higher amount of provided energy. Such behavior has, however, an asymptotical trend, as it only manifested after an increment in temperature of 350 °C for 1 h.

The XRD patterns of both the CB and CB/GO samples in all the examined temperature conditions are depicted in Figure 3b. They all show the two main features of amorphous carbons: the (002) reflection at around 22.63° and the (10) reflection at around 43.66°. The first is a characteristic of carbon lattices and appears downshifted from the 26.38° of the more ordered graphite, leading to a larger interplanar spacing d_{002} (in accordance with Bragg's law expressed in Equation 1). The second arises instead from the merging of the (100) and (101) carbon lattice peaks, usually shown at 42.22° and 44.39° respectively, due to the turbostratic arrangements of graphene layers (Krishnankutty, Vannice, 1995). Using the Scherrer formula expressed in Equation 2, it is possible to calculate the stacking height L_C, from the (002) peak and with a shape factor of 0.89, and the crystallite lateral size L_A, from the (10) peak and with a shape factor of 1.84 (Biscoe, Warren, 1942). The results from previous calculations are summarized in Table 1. From the latter it is possible to observe how d_{002} in CB samples is similar when subjected to ambient drying and thermally treatment at 550 °C, while it's larger when thermally treated at 200 °C. When GO is introduced, d_{002} is larger for the AD sample, larger also when compared to CB only, comparable in size in CB/GO_TT_200 and highly contracted in CB/GO_TT_550, with a value that is even smaller than CB_TT_550. Accordingly, L_C shows a similar trend. Regarding L_A, in CB samples it decreases from AD to the treatment at 200 °C and then it increases again in CB_TT_550; when GO is introduced, L_A instead increases from CB/GO_AD to CB/GO_TT_200 and then slightly decreases after the treatment at 550 °C. Such behavior is explainable with the intercalation of GO sheets that initially leads to more expanded and disordered stackings and then, when the complete reduction to rGO thanks to the treatment at 550 °C occurs, they promote instead higher compaction and order. Summarizing, XRD shows a U-trend of the structure optimization for rising temperatures. In accordance with Mitsuda et al., a critical temperature of 310 °C for a minimum of 30 min under inert atmosphere is required for the complete evaporation of TX100. A non-complete evaporation and partial degradation of the latter could thus explain the results after the treatment at 200 °C and the trend previously described.

Table 1: Raman D to G band ratios, XRD Peak Positions, Lattice Spacing and Crystallite Sizes.

Sample	I_D/I_G ratio	(002), 2ϑ	(10), 2ϑ	d_{002}, Å	L_C, Å	L_A, Å
CB_AD	1.07	23.01	43.63	3.86	18.6	40.4
CB/GO_AD	0.97	22.23	43.7	4.00	27.3	36.3
CB_TT_200	1.07	21.92	43.74	4.05	30.4	36.0
CB/GO_ TT_200	1.05	22.00	43.65	4.04	28.1	41.6
CB_TT_550	1.07	23.09	43.63	3.85	18.1	42.1
CB/GO_ TT_550	1.04	23.55	43.60	3.77	17.8	41.0

3.3 Zeta potential

The ζ-potential or Zeta Potential (*ZP*) analysis is a technique used to estimate the surface charge of particles dispersed in a solvent. An electric field causes a motion of charged particles and the formation of a charged layer, consisting of solvent molecules, around them: *ZP* is the voltage difference between this layer and the outer part of the solvent (the interface is called slipping plane). In the case of GO in water, the *ZP* is -48.3 mV, meaning that GO flakes are rich of negative charges due to oxygen-containing groups, explaining then its hydrophilicity and stability in water. After the thermal treatment at 550°C, the *ZP* becomes -7.51 mV. This value indicates a strong reduction of the negative surface charge, accordingly with GO reduction. Figure 3b shows the *ZP* Distributions (*ZPD*) of GO and of GO_TT_550. In particular, the GO ZPD has a wide feature formed by a main peak at -44.8 mV and by a second peak at -60.3 mV, with standard deviations of 6.42 and 4.45 respectively. GO_TT_550 ZPD has instead only one sharp peak with standard deviation of 3.68 mV. A comparison between the ZPDs remarks the GO reduction efficacy due to the thermal treatment considering its uniformity over the GO particles, regardless their initial level of oxidation.
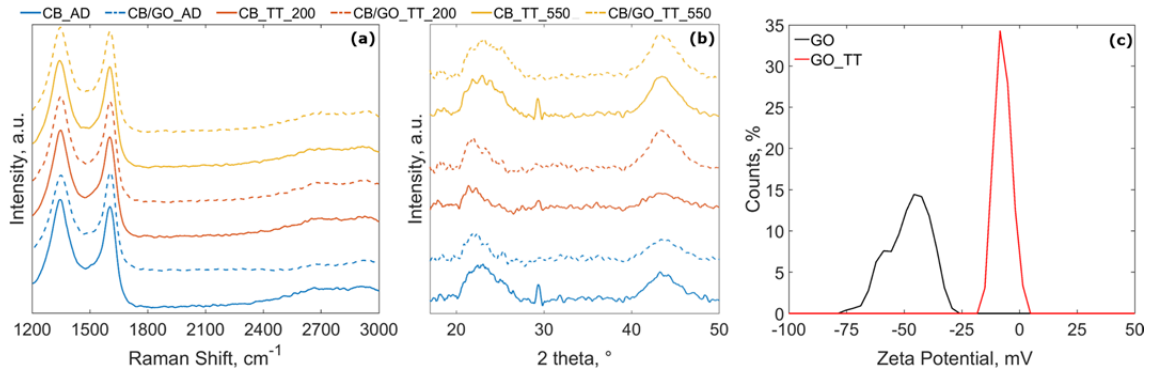
Figure 3: (a) Raman spectra and (b) XRD patterns of all the samples; (c) Zeta Potential Distribution (in terms of percentage of counts) of GO and GO_TT.

3.4 Chemical kinetics hypothesis

As previously shown in this work, the GO reduction reaction can be observed with different characterization techniques. However, in order to quantitatively evaluate it, additional hypotheses are required. The final purpose is an estimation of the reduction degree, i.e. the mole ratio of oxygen presence in the molecules before and after the thermal treatment, which lacked in our previous work (Rapisarda et al., 2020). Particularly, the results from the ZP analysis can be used under the hypothesis of validity of the following formula, conceived by Ge and Wang (2017) for a similar purpose:

$$\sigma_{eff} = \sqrt{8cN\epsilon_r\epsilon_0 k_B T}\,\sinh\left(\frac{e\zeta}{2k_B T}\right) \tag{4}$$

where σ_{eff} is the effective surface charge density (the sum of charge density on a flat surface and its surrounding ions enclosed by the slipping plane), T is the absolute temperature (298.15 K; i.e., the 25 °C of the ζ-analysis) while all the other parameters, whose nature is beyond the scope of this estimation, are constant since both GO and GO_TT were dispersed in the same solvent at the same condition. Since *ZP* changed after the thermal treatment, the ratio of σ_{eff} before and after the reaction gives an estimate of the remaining charges on GO after reduction. Using data from the as performed ZP analysis, the resulting ratio is of 0.135, meaning that GO_TT lost the 86.5 % of the initial oxygen-containing groups.

At this stage, it is then possible to proceed with a chemical kinetics evaluation. Assuming that the GO reduction evolution can be described with the following law (5):

$$n_O(\mathrm{t}) = n_O(0)e^{-t/\tau} \tag{5}$$

where $n_O(t)$ is the mole number at the time *t*, $n_O(0)$ the initial mole number and τ the time constant at fixed temperature. In fact, using the estimated ratio from the previous calculation at *t* of 1,800 s, the value of 900 s can be derived from (5) for τ. This means that the adopted 30 min treatment corresponds to a GO reduction after 2τ, while a 60 min one would correspond to a 4τ reduction. The latter is beyond 3.5τ, that is the time used as a practice for the phenomena governed by a negative exponential trend. Thermal treatments duration between 30 and 60 min are hence recommended for an efficient GO reduction during SCs electrode fabrication, as: higher temperatures (i.e. minor time) are too close to the melting point of aluminum, that is the most commonly used current collector, while at lower temperatures the required reaction time for an effective reduction grows exponentially due to the inherent dependence of τ from temperature. In other word, the kinetic analysis evidenced a time optimization congruent with the temperature optimization.

4. Conclusions

This work shows how the temperature can be a crucial parameter for a multifactorial optimization problem. With the aim of drying the described water-based slurry consisting of a CB/GO nanocomposite during SCs electrodes fabrication, the minimum temperature is the highest between the boiling points of the solvent (i.e., 100 °C for water) and the used non-conductive surfactant additives (i.e., 270 °C for TX100). However, at 550 °C, that is close to the maximum temperature that the electrode could withstand, the GO reduction takes place at its chemical-kinetic limits and improvement of the nanocomposite structure were evidenced by the chemical-physical analysis. Finally, considering also time as a factor for an industrial scale-up, the analysis

suggests that performing the thermal treatment at the limit temperature of 550 °C, even though implying higher energy costs, allows a better optimization of the manufacturing process.

Acknowledgments

References

ASTM D3053-20a, Standard Terminology Relating to Carbon Black, ASTM International, West Conshohocken, PA, 2020, www.astm.org.

Biscoe J., Warren B. E.,1942, An X-Ray Study of Carbon Black. Journal of Applied Physics, 13(6), 364–371.

Bragg W. H., Bragg W. L., 1913, The reflection of X-rays by crystals. Proceedings of the Royal Society of London. Series A, Containing Papers of a Mathematical and Physical Character, 88(605), 428–438.

Carmo M., dos Santos A. R., Poco J. G. R., Linardi M., 2007, Journal of Power Sources, 173, 860–866.

Ferrari, A. C., 2007, Raman spectroscopy of graphene and graphite: Disorder, electron–phonon coupling, doping and nonadiabatic effects, Solid State Communications, 143(1), 47–57.

Frackowiak E., Beguin F., 2001, Carbon materials for the electrochemical storage of energy in capacitors, Carbon, 39, 937–950.

Delgado A. V., González-Caballero F., Hunter R. J.; Koopal L. K., Lyklema J., 2005, Measurement and Interpretation of Electrokinetic Phenomena (IUPAC Technical Report), Pure and Applied Chemistry, 77(10), 1753–1805.

Ge Z., Wang Y., 2017, Estimation of Nanodiamond Surface Charge Density from Zeta Potential and Molecular Dynamics Simulations, The Journal of Physical Chemistry B, 121, 3394–3402.

Henry D. C., 1931, The cataphoresis of suspended particles. Part I. – The equation of cataphoresis, Proceeding of the Royal Society A, 133, 106–129.

Jeong H.-K., Lee Y. P., Jin M. H., Kim, E. S., Bae, J. J., Lee, Y. H., 2009, Thermal stability of graphite oxide, Chemical Physics Letters, 470 (4), 255–258.

Ke Q., Wang J., 2016, Graphene-based materials for supercapacitor electrodes – A review, Journal of Materiomics, 2(1), 37–54.

Krishnankutty N., Vannice M. A., 1995, Effect of Pretreatment on Surface Area, Porosity, and Adsorption Properties of a Carbon Black, Chemistry of Materials, 7(4), 754–763.

Mitsuda K., Kimura H., Murahashi T., 1989, Evaporation and decomposition of Triton X-100 under various gases and temperatures, Journal of Materials Science, 24(2), 413–419.

Pei S., Zhao J., Du J., Ren W., Cheng H.-M., 2010, Direct reduction of graphene oxide films into highly conductive and flexible graphene films by hydrohalic acids, Carbon, 48, 4466–4474.

Pimenta, M. A., Dresselhaus, G., Dresselhaus, M. S., Cançado, L. G., Jorio, A., Saito, R., 2007, Studying disorder in graphite-based systems by Raman spectroscopy, Physical Chemistry Chemical Physics, 9(11), 1276–1290.

Rapisarda M., Damasco A., Abbate G., Meo M., 2020, Carbon Black and Reduced Graphene Oxide Nanocomposite for binder free supercapacitors with Reduced Graphene Oxide Paper as current collector, ACS Omega, 5(50), 32426–32435.

Scherrer P., 1918, Bestimmung der Größe und der inneren Struktur von Kolloidteilchen mittels Röntgenstrahlen. Nachrichten von der Gesellschaft der Wissenschaften zu Göttingen, Mathematisch-Physikalische Klasse, 98–100.

Schniepp, H. C., Li, J.-L., McAllister, M. J., Sai, H., Herrera-Alonso, M., Adamson, D. H., Prud'homme, R. K., Car, R., Saville, D. A., Aksay, I. A., 2006, Functionalized Single Graphene Sheets Derived from Splitting Graphite Oxide, The Journal of Physical Chemistry B, 110(17), 8535–8539.

Stobinski L., Lesiak B., Malolepszy A., Mazurkiewicz M., Mierzwa B., Zemek J., Jiricek P., Bieloshapka I., 2014, Graphene oxide and reduced graphene oxide studied by the XRD, TEM and electron spectroscopy methods, Journal of Electron Spectroscopy and Related Phenomena, 145–154.